International Journal of Damage Mechanics

http://ijd.sagepub.com

Over-leg Bending Test for Mixed-mode I/II Interlaminar Fracture in Composite Laminates

András Szekrényes and József UJ

The online version of this article can be found at:
http://ijd.sagepub.com/cgi/content/abstract/16/1/5

Additional services and information for *International Journal of Damage Mechanics* can be found at:

Email Alerts: http://ijd.sagepub.com/cgi/alerts

Subscriptions: http://ijd.sagepub.com/subscriptions

Reprints: http://www.sagepub.com/journalsReprints.nav

Permissions: http://www.sagepub.com/journalsPermissions.nav

Over-leg Bending Test for Mixed-mode I/II Interlaminar Fracture in Composite Laminates

ANDRÁS SZEKRÉNYES* AND JÓZSEF UJ

Department of Applied Mechanics, Budapest University of Technology and Economics, Budapest, PoB 11, H-1521, Hungary

ABSTRACT: In this work the over-leg bending (OLB) specimen is developed for mixed-mode I/II delamination characterization in composites. The traditional single-leg bending (SLB) specimen is modified by introducing the load eccentrically between the two supports of a three-point bending setup. The modified configuration is analyzed by using linear beam theories. The theories of transverse shear, Winkler-Pasternak-type elastic foundation, Saint-Venant effect, and crack tip shear deformation are incorporated in the analysis. Also, experiments are carried out on glass/polyester unidirectional specimens. Comparison between the results of analysis and experiment shows very good agreement. The traditional SLB and the novel OLB coupons are compared, and their advantages and drawbacks are highlighted. The newly developed OLB setup is relatively easier to perform and crack propagation may be simply investigated under displacement control.

KEY WORDS: composite delamination, beam theory, mode-mixity, fracture, SLB specimen, OLB specimen.

INTRODUCTION

THE INTERLAMINAR FRACTURE tests play an important role in the design and development of composite structures. Usually, these tests are performed by using specimens, which may be considered as slender beams. The double-cantilever beam (DCB) (Olsson, 1992; Yang and Sun, 2000; Morais et al., 2002) specimen is a standard tool to measure the mode-I fracture in composite materials.

*Author to whom correspondence should be addressed. E-mail: szeki@mm.bme.hu
Figures 7 and 14 appear in color online: http://ijd.sagepub.com

For mode-II testing, six specimens are available. The end-notched flexure (ENF) (Carlsson et al., 1986; Ozdil and Carlsson, 1998) is the subject in most of the works. In contrast, its stabilized form (SENF) was discussed only in a few works (e.g., Davies et al., 1996). The four-point bend end-notched flexure (4ENF) test is also a popular geometry (Schuecker and Davidson, 2000; Davies et al., 2004). Another candidate for mode-II fracture investigation is the end-loaded split (ELS) coupon (Hashemi et al., 1990a, b; Wang and Vu-Khanh, 1996). The over-notched flexure (ONF) specimen (Tanaka et al., 1998; Wang et al., 2003; Szekrényes and Uj, 2005b) is the modified version of the ENF one. The only difference between them is that in the ONF setup the load is introduced eccentrically between the two supports of the three-point bending apparatus. More recently, the tapered end-notched flexure (TENF) specimen was proposed by Wang and Qiao (2003) and Qiao et al. (2004). A remarkable feature is that in the case of a proper design the compliance rate change is independent of the crack length, which is useful, for instance in the case of carbon-fiber reinforced systems, when the crack length is difficult to measure accurately. All these specimens have advantages and relative drawbacks (Davies et al., 1996; Szekrényes and Uj, 2005b).

In the case of the mixed-mode I/II delamination, the number of different specimens is particularly high. The single-cantilever beam (SCB) (or known as the mixed-mode ELS specimen) requires a clamping fixture (Hashemi et al., 1990a, b). The simple single-leg bending (SLB) specimen was proposed by Yoon and Hong (1990) as a modified ENF test, although an earlier paper on this type of delamination specimen was published by Russel and Street (1985). The mixed-mode flexure (MMF) is quite similar to the SLB test. It is also a common setup for mixed-mode testing (Albertsen et al., 1995; Korjakin et al., 1998). A remarkable feature is that they may be performed in a three-point bending fixture. The cracked-lap shear (CLS) specimen (e.g., Albertsen et al., 1995) was also an attempt, although it did not become an optimal solution due to certain complications. The asymmetric double-cantilever beam (ADCB) (Bradley and Cohen, 1985) was able to vary the mode-ratio, but it required a complex loading system, therefore it was also abandoned. The standard mixed-mode bending (MMB, ASTM D6671-01) specimen was developed by Reeder and Crews (1990). It is the most universal mixed–mode setup (Ozdil and Carlsson, 1999; Ducept et al., 1999), although it is widely accepted mainly for testing of unidirectional coupons. In addition, it requires a complex fixture, bonded steel hinged tabs and a complex beam theory-based reduction technique. In some cases, for example in angle-ply or multidirectional MMB specimens, discrepancies between manufactured and predicted bending stiffnesses may give misleading results. Hence, the researchers also use other types of mixed-mode configurations.

Davidson et al. performed extensive theoretical and experimental works using SLB coupons (Davidson et al., 1995, 1996, 1997, 1999, 2000). This type of specimen was also investigated by Polaha et al. (1996) and Pieracci et al. (1998). Later, the SLB test was modified by Tracy et al. and the single-leg four point bend (SLFPB) geometry was introduced (Tracy et al., 2003). In the current study we developed another alternative: the over-leg bending (OLB) specimen.

In general the fracture specimens are treated as slender beams. There are several analytical solutions, which are based on beam and plate models. The solution by Reeder and Crews (1990), or Ozdil and Carlsson (1999) for the MMB specimen and Olsson for the DCB specimen (Olsson, 1992) are based on the elastic foundation model by Williams (1989). There were many efforts to derive a correction also for mode-II specimens. See for instance the works by Carlsson et al. (1986), Chatterje (1991), and Ding and Kortschot (1999). None of these solutions were satisfactory. This void was addressed by Wang and Qiao (2004a), who presented an improved solution for the mode-II ENF specimen, which had a similar form to that of the elastic foundation model by Williams (1989).

The mode-mixity is also an important issue in interlaminar fracture problems. Williams' global method (Williams, 1988) is the simplest. A more accurate local method was developed by Suo and Hutchinson (1990). The global and local methods give the same result if the delamination is symmetrically located along the beam thickness and the upper and lower arms have the same mechanical properties. Later, the local method was completed with the effect of shear forces by Wang and Qiao (2004b), who also presented generalized solutions using the concept of the elastic foundation model and the crack tip deformation theory (Qiao and Wang, 2004). A beam theory-based analytical delamination model was also presented by Szekrényes and Uj (2004, 2005c) incorporating Williams' global approach, and comparison was made with some of the existing models (Szekrényes and Uj, 2005a). It should be mentioned that the energy release rates calculated by the global approach are not the same as the conventional definitions of the energy release rates (Tay, 2003). On the other hand, it is also unclear how it could be applied to composite structures, in general (Pagano and Schoeppner, 2000). In spite of that, the authors apply the global method in their case as the simplest solution can be obtained this way.

As a continuation of these works the authors propose the novel OLB configuration. The novel specimen is analyzed based on linear beam theories and experiments. A comparative study is made between the OLB and the traditional SLB configurations. Finally, there is some discussion on the obtained results. The OLB specimen is able to investigate the mixed-mode crack propagation in composites with low flexural modulus,

and the crack propagation is easy to control. Furthermore, a simple reduction technique can be applied to reduce the experimental data.

BEAM THEORY-BASED ANALYSIS

The SLB and OLB mixed-mode I/II delamination coupons are shown in Figure 1. The fracture properties of the specimens are calculated based on previous works. The expressions incorporate transverse shear analysis (Ozdil and Carlsson, 1998), Saint-Venant (SV) effect (Olsson, 1992), Winkler-Pasternak-type elastic foundation (Szekrényes and Uj, 2004, 2005c), and crack tip shear deformation analysis (Wang and Qiao, 2004a). For the sake of completeness, we give a brief summary on the applied models and theories. Usually, the application of the Euler–Bernoulli (EB) and Timoshenko (TIM) beam theories are not too complicated, and for the common fracture specimens the compliance and strain energy release rate (SERR) expressions are known. Consequently, the compliance and strain energy release rate may be obtained in a fashion similar to that shown for instance in Ozdil and Carlsson (1998) or Szekrényes and Uj (2004). The compliance and the strain energy release rate of the SLB specimen shown in Figure 1(a) is (Szekrényes and Uj, 2004):

$$C^{\mathrm{SLB}} = C_{\mathrm{EB}}^{\mathrm{SLB}} + C_{\mathrm{TIM}}^{\mathrm{SLB}} = \frac{7a^3 + 2L^3}{8bh^3 E_{11}} + \frac{a + 2L}{8bhkG_{13}}, \tag{1}$$
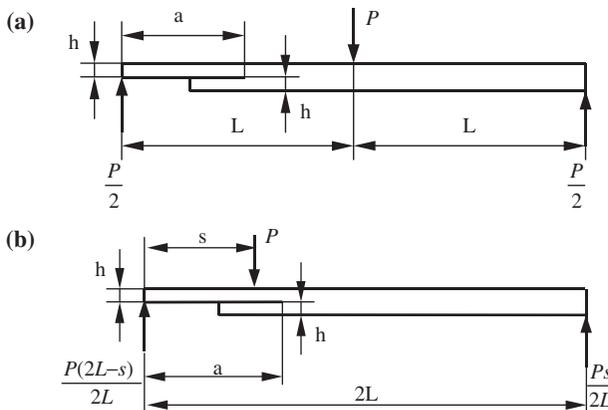
Figure 1. *Delamination specimens: (a) The single-leg bending (SLB) and (b) the over-leg bending (OLB).*

where the first term is the result of the EB beam theory and the second one is from TIM beam theory. The strain energy release rate may be obtained by using the Irwin-Kies expression (e.g., Olsson, 1992):

$$G_{\text{I/II}} = \frac{P^2}{2b}\frac{dC}{da}, \tag{2}$$

i.e., we have:

$$G_{\text{I/II}}^{\text{SLB}} = \frac{21P^2a^2}{16b^2h^3E_{11}} + \frac{P^2a^2}{16b^2h^3E_{11}}f_{\text{T}}, \tag{3}$$

where

$$f_{\text{T}} = \frac{1}{k}\frac{E_{11}}{G_{13}}\left(\frac{h}{a}\right)^2. \tag{4}$$

The compliance of the OLB specimen can be obtained by performing a similar analysis (incorporating E-B and TIM beam theory) to that in Ozdil and Carlsson (1998) or Szekrényes and Uj (2004):

$$
\begin{aligned}
C^{\text{OLB}} &= C_{\text{EB}}^{\text{OLB}} + C_{\text{TIM}}^{\text{OLB}} \\
&= \frac{s^2c^3}{8bh^3E_{11}L^2}\left[1 + 8\frac{a}{c} + 16\frac{aL}{c^2} + 32\frac{aL^2}{c^3} + 16\frac{Ls(s-4L)}{c^3}\right] \\
&\quad + \frac{s[4L(2L-s)]}{8bhkG_{13}L^2}.
\end{aligned}
\tag{5}
$$

The SERR can be calculated combining Equations (2) and (5):

$$G_{\text{I/II}}^{\text{OLB}} = \frac{21P^2s^2c^2}{16b^2h^3E_{11}L^2} + \frac{P^2s^2c^2}{16b^2h^3E_{11}L^2}f_{\text{T}}. \tag{6}$$

In Equations (1)–(6) a is the crack length, L is the half span length, b is the specimen width, h is half of the specimen thickness, $c = 2L - a$ is the length of the uncracked region, $k = 5/6$ is the shear correction factor, E_{11} is the flexural modulus, E_{33} is the through-thickness modulus, G_{13} is the shear modulus of the material and P is the external force required for crack initiation/propagation. We note again that these equations contain only the contribution of EB and TIM beam theory. Furthermore, the individual mode components (G_{I} and G_{II}) are not yet determined.

Winkler-Pasternak Foundation Analysis

The effect of the two-parameter elastic foundation was studied in our previous work (Szekrényes and Uj, 2005c). Here we summarize the result of the analysis. Let us consider the general loading scheme depicted in Figure 2. The model has four deflection functions. Two of them are EB beams (cracked region), while in the uncracked portion the beam is mounted on an elastic foundation. The analysis was performed according to the following:

- The governing differential equations of the uncracked portion were formulated by using the variational formulation of the potential energy.
- The coefficients in the differential equations were determined and were related to the elastic properties of the material.
- The solution functions of the uncracked region were found in the form of the combination of hyperbolic functions, the cracked region was modeled as EB beams.
- The continuity and boundary conditions were formulated and the coefficients of the deflection functions were determined.
- The compliance of both arms in the model was determined by taking the deflection at the point of load applications.

The solution resulted in the following expressions for the compliances of the upper (1) and lower (2) arms:

$$C_{\mathrm{WP1}} = \frac{7a^3 + L^3}{2bh^3 E_{11}} + \frac{(L^3 - a^3)P_2}{2bh^3 E_{11} P_1} + \frac{a^3(P_1 - P_2)}{2bh^3 E_{11} P_1} f_{\mathrm{W1}}, \tag{7}$$

$$C_{\mathrm{WP2}} = \frac{7a^3 + L^3}{2bh^3 E_{11}} + \frac{(L^3 - a^3)P_1}{2bh^3 E_{11} P_2} + \frac{a^3(P_1 - P_2)}{2bh^3 E_{11} P_2} f_{\mathrm{W1}}, \tag{8}$$
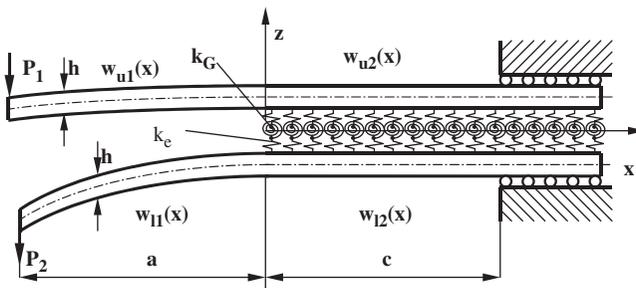
Figure 2. Two-parameter elastic foundation model.

where

$$f_{W1} = 2.71\phi^{1/2}\left(\frac{h}{a}\right)\left(\frac{E_{11}}{E_{33}}\right)^{1/4} + 2.45\phi\left(\frac{h}{a}\right)^2\left(\frac{E_{11}}{E_{33}}\right)^{1/2} + 1.11\phi^{1/2}\left(\frac{h}{a}\right)^3\left(\frac{E_{11}}{E_{33}}\right)^{3/4},$$

(9)

where $\phi = 1 + \omega$, and ω is a parameter related to the Pasternak-type foundation. A series of FE analyses on composite specimens with different material properties resulted in $\omega = 2.5$, which may be considered as a constant (Szekrényes and Uj, 2005c). The first two terms in Equations (7) and (8) are the result of the EB beam theory, while the third one is the correction based on the two-parameter elastic foundation. The energy release rates for the upper and lower arms may be obtained by using Equation (2):

$$G_1 = \frac{P_1^2}{2b}\frac{dC_1}{da}, \quad G_2 = \frac{P_2^2}{2b}\frac{dC_2}{da}.$$

(10)

Thus, we may obtain:

$$G_{WP1} + G_{WP2} = \frac{21\left(P_1^2 + P_2^2\right)a^2}{4b^2h^3E_{11}} - \frac{6P_1P_2a^2}{4b^2h^3E_{11}} + \frac{(P_1 - P_2)^2 a^2}{4b^2h^3E_{11}}f_{W2},$$

(11)

where,

$$f_{W2} = 5.42\phi^{1/2}\left(\frac{h}{a}\right)\left(\frac{E_{11}}{E_{33}}\right)^{1/4} + 2.45\phi\left(\frac{h}{a}\right)^2\left(\frac{E_{11}}{E_{33}}\right)^{1/2}$$

(12)

Note that the result of the Winkler foundation model may be recovered by using $\omega = 0$ in Equations (9) and (12) (Szekrényes and Uj, 2004).

Saint-Venant Effect at the Crack Tip

The SV effect means a rotational angle at the crack tip due to bending moments. This effect is essentially related to the mode-I component. According to Olsson's analysis (1992), the strain energy derivative in the coordinate system in Figure 3 is bounded by the following inequality:

$$\frac{\partial U}{\partial x} \leq 2\frac{\partial U}{\partial x}\bigg|_0 e^{-2x/\kappa}, \quad \kappa = \frac{h}{2\pi}\left(\frac{E_{11}}{G_{13}}\right)^{1/2},$$

(13)
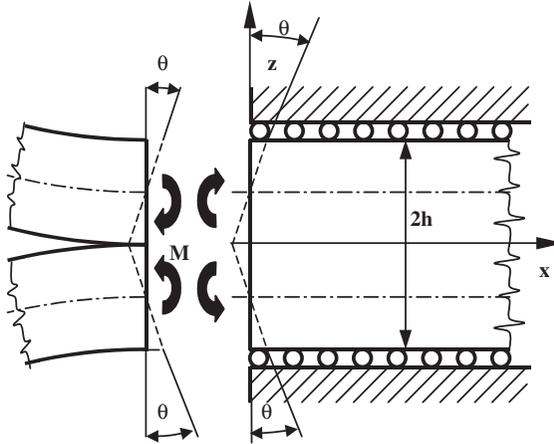
Figure 3. *Saint-Venant effect at the crack tip.*

where κ is the characteristic decay length in the material. This means that the strain energy related to the SV effect decays exponentially ahead of the crack tip. A relevant analysis resulted in the following compliance contributions from the upper and lower arms (Szekrényes and Uj, 2005c):

$$C_{SV1} = C_{SV2} = \frac{6}{\pi} \frac{a^2}{bh^2 E_{11}} \left(\frac{E_{11}}{G_{13}}\right)^{1/2},$$ (14)

It has been shown that the energy release rate caused by the Saint-Venant effect may be written as (Szekrényes and Uj, 2005c):

$$G_{SV} = \frac{(P_1 - P_2)^2 a^2}{4b^2 h^3 E_{11}} f_{SV},$$ (15)

where,

$$f_{SV} = \frac{12}{\pi} \left(\frac{h}{a}\right) \left(\frac{E_{11}}{G_{13}}\right)^{1/2}.$$ (16)

Crack Tip Shear Deformation Analysis

The concept of crack tip shear deformation was originally provided by Wang and Qiao (2004a). Their solution was adopted in our last works
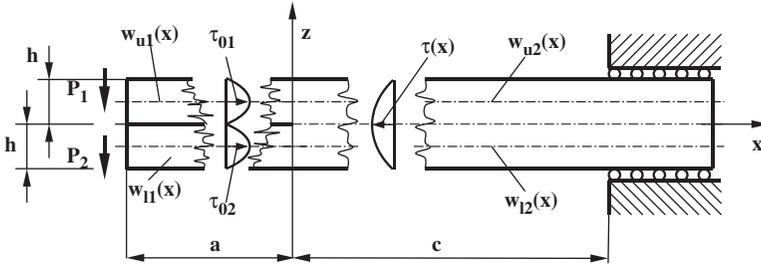
Figure 4. *Loading scheme for the crack tip deformation analysis.*

(Szekrényes and Uj, 2005b, 2005c), wherein the same concept was used to obtain the solution of the general model depicted in Figure 4. Again, we give only a short description on the results obtained:

- The shear stress field (τ (x)) and the deflections of the beam in Figure 4 were determined by following the way suggested by Wang and Qiao (2004a)
- The continuity and boundary conditions were also formulated, the coefficients of the deflection functions were determined
- The compliance of both arms of the model was determined by taking the deflection at the point of load application.

After some simplifications the analysis resulted in the following compliance contributions:

$$C_{\text{SH1}} = \frac{w_{\text{u1}}(-a)}{P_1} = \frac{(P_1 + P_2)a^3}{2P_1 bh^3 E_{11}} f_{\text{SH1}}, \tag{17}$$

$$C_{\text{SH2}} = \frac{w_{\text{l1}}(-a)}{P_2} = \frac{(P_1 + P_2)a^3}{2P_2 bh^3 E_{11}} f_{\text{SH1}}, \tag{18}$$

where,

$$f_{\text{SH1}} = 0.98 \left(\frac{h}{a}\right) \left(\frac{E_{11}}{G_{13}}\right)^{1/2} + 0.43 \left(\frac{h}{a}\right)^2 \left(\frac{E_{11}}{G_{13}}\right). \tag{19}$$

The SERR for the upper and lower arms by using Equation (10) are:

$$G_{\text{SH1}} + G_{\text{SH2}} = \frac{(P_1 + P_2)^2 a^3}{4b^2 h^3 E_{11}} f_{\text{SH2}}, \tag{20}$$

where,

$$f_{SH2} = 1.96\left(\frac{h}{a}\right)\left(\frac{E_{11}}{G_{13}}\right)^{1/2} + 0.43\left(\frac{h}{a}\right)^2\left(\frac{E_{11}}{G_{13}}\right). \tag{21}$$

Mode-mixity Analysis

According to Figure 5 the authors reduce problem (a) into problem (b), wherein the effect of Winkler-Pasternak foundation, transverse shear, SV and crack tip shear deformation are incorporated. In Figure 5 $M_1 = P_1 a$, $M_2 = P_2 a$, and $M_3 = M_1 + M_2$ are bending moments at the crack tip. The sum of Equations (11), (15), and (20) can be transformed as:

$$G_T = \frac{21\left(M_1^2 + M_2^2\right) - 6M_1 M_2 + (M_1 - M_2)^2(f_{W2} + f_{SV}) + (M_1 + M_2)^2 f_{SH2}}{4b^2 h^3 E_{11}}. \tag{22}$$

The authors assume that the equivalent bending moments can be decomposed as follows (Williams, 1988):

$$M_1 = M_I + M_{II}, \quad M_2 = \alpha M_I + \varphi M_{II}. \tag{23}$$
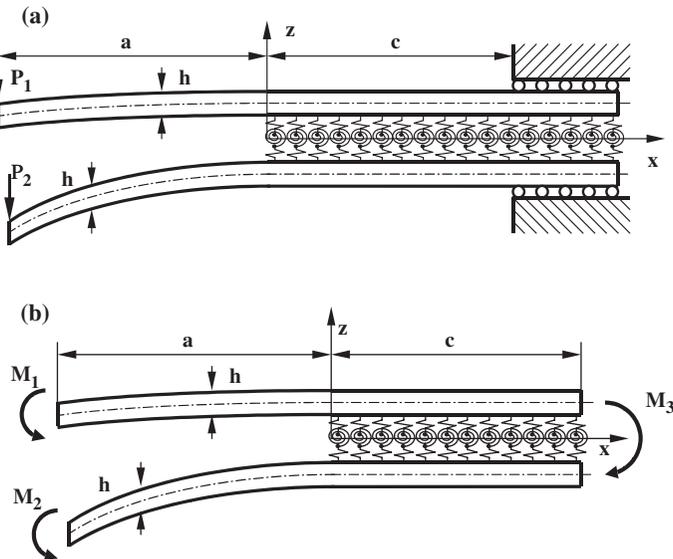
Figure 5. Reduction scheme for mixed-mode partitioning. Original problem (a). Reduced problem (b).

Substituting Equation (23) into Equation (22) the total SERR are obtained in the form of:

$$G_T = G_I + G_{II} + G_{I+II}^*, \tag{24}$$

where G_I and G_{II} are the individual mode-I and mode-II SERR components, G_{I+II}^* is a term, which contains the product of $M_I \cdot M_{II}$. The last term should be eliminated. Williams (1988) supposes that in the case of pure mode-II the upper and lower specimen arms have the same curvature:

$$\frac{12 M_{II}}{b h^3 E_{11}} = \frac{12 \varphi M_{II}}{b h^3 E_{11}}. \tag{25}$$

From this beam kinematics assumption it follows that $\varphi = 1$. Substituting Equation (23) into Equation (22) the term containing the product of $M_I \cdot M_{II}$ can be separated:

$$G_{I+II}^* = \frac{(9 + f_{SH2}) M_I M_{II} (1 + \alpha)}{b^2 h^3 E_{11}}. \tag{26}$$

In order to cancel Equation (26) we choose $\alpha = -1$. Referring to (Szekrényes and Uj, 2004), wherein it has been found that the transverse shear (f_T) contributes only to the mode-I component, and from Equations (22) and (23), the mode-I and mode-II components become:

$$G_I = \frac{M_I^2 (12 + f_{W2} + f_T + f_{SV})}{b^2 h^3 E_{11}}, \tag{27}$$

$$G_{II} = \frac{M_{II}^2 (9 + f_{SH2})}{b^2 h^3 E_{11}}. \tag{28}$$

Rearranging Equation (23) the mode-I and mode-II bending moments are obtained as follows:

$$M_I = \frac{M_1 - M_2}{2}, \quad M_{II} = \frac{M_1 + M_2}{2}. \tag{29}$$

where f_{W2} is given by Equation (12), f_T is given by Equation (4), f_{SV} is defined by Equation (16) and f_{SH2} is defined by Equation (21).

Compliance Calculation

The authors give a general expression, which can be applied to calculate the compliance for a beam under general loading condition. In a general form the mode-I and mode-II bending moments (Equation (29)) may be written as:

$$M_I = P \cdot f_I \cdot a^*, \quad M_{II} = P \cdot f_{II} \cdot a^*, \tag{30}$$

where P is the external load, f_I and f_{II} are related to geometrical parameters of the system and a^* is the characteristic length (in each case may be related to the crack length). As it was shown, the two-parameter elastic foundation and SV effect contribute only to the mode-I component, while the crack tip shear deformation improves only the mode-II SERR. Therefore, in a general form the compliance of delaminated beams may be obtained as:

$$C = C_{EB} + C_{TIM} + \frac{f_I^2 a^3}{2bh^3 E_{11}} \left(\frac{f_{SV}}{2} + f_{W1} \right) + \frac{f_{II}^2 a^3}{2bh^3 E_{11}} f_{SH1}, \tag{31}$$

where the determination of the terms C_{EB} and C_{TIM} requires a unique analysis. Moreover, f_{W1} is given by Equation (9), f_{SV} is defined by Equation (16) and f_{SH1} is defined by Equation (19). The application of Equations (27), (28), and (31) will be demonstrated in the next section.

Application to the SLB and OLB Specimens

Let us consider the case of the SLB specimen in Figure 1(a), where $M_1 = Pa/2$ and $M_2 = 0$. From Equation (29) it follows that $M_I = M_{II} = Pa/4$. Furthermore, comparing Equation (29) to (30) we may establish that $f_I = f_{II} = 1/4$ and $a^* = a$. Substituting these into Equation (31) and also using Equation (1), the following expression for the compliance of the SLB specimen are obtained:

$$C^{SLB} = \frac{7a^3 + 2L^3}{8bh^3 E_{11}} + \frac{a + 2L}{8bhkG_{13}} + \frac{a^3}{8bh^3 E_{11}} \left[0.98 \left(\frac{h}{a} \right) \left(\frac{E_{11}}{G_{13}} \right)^{1/2} + 0.43 \left(\frac{h}{a} \right)^2 \left(\frac{E_{11}}{G_{13}} \right) \right]$$

$$+ \frac{1}{\pi} \frac{3a^2}{4bh^2 E_{11}} \left(\frac{E_{11}}{G_{13}} \right)^{1/2} + \frac{a^3}{8bh^3 E_{11}} \left[5.07 \left(\frac{h}{a} \right) \left(\frac{E_{11}}{E_{33}} \right)^{1/4} + 8.58 \left(\frac{h}{a} \right)^2 \left(\frac{E_{11}}{E_{33}} \right)^{1/2} \right.$$

$$\left. + 2.08 \left(\frac{h}{a} \right)^3 \left(\frac{E_{11}}{E_{33}} \right)^{3/4} \right], \tag{32}$$

where the first two terms are given by Equation (1), the third is from the crack tip shear deformation, the fourth captures the SV effect, while the last term is the effect of the Winkler-Pasternak foundation. Also, using Equations (27) and (28) with the aid of the aforementioned moments (M_I, M_{II}), the following is obtained:

$$G_I^{SLB} = \frac{12P^2a^2}{16b^2h^3E_{11}}\left[1 + 0.85\left(\frac{h}{a}\right)\left(\frac{E_{11}}{E_{33}}\right)^{1/4} + 0.71\left(\frac{h}{a}\right)^2\left(\frac{E_{11}}{E_{33}}\right)^{1/2}\right.$$

$$\left. + 0.32\left(\frac{h}{a}\right)\left(\frac{E_{11}}{G_{13}}\right)^{1/2} + 0.1\left(\frac{h}{a}\right)^2\left(\frac{E_{11}}{G_{13}}\right)\right], \quad (33)$$

$$G_{II}^{SLB} = \frac{9P^2a^2}{16b^2h^3E_{11}}\left[1 + 0.22\left(\frac{h}{a}\right)\left(\frac{E_{11}}{G_{13}}\right)^{1/2} + 0.048\left(\frac{h}{a}\right)^2\left(\frac{E_{11}}{G_{13}}\right)\right]. \quad (34)$$

In what follows, the compliance and the energy release rate of the OLB specimen are calculated. In this case it may be written that $M_1 = Ps(2L-a)/2L$ and $M_2 = 0$ (Figure 1(b)). From Equation (29) it follows that $M_I = M_{II} = Ps(2L-a)/4L$. Comparing Equations (29) and (30) that it is concluded $f_I = f_{II} = s/4L$ and $a^* = 2L - a$. This means that the crack length 'a' in Equations (4), (9), (12), (16), (19) and (21) should be replaced with $2L - a$. Substituting $2L - a$ with c in Equation (31) and also incorporating Equation (4) the following is obtained:

$$C^{OLB} = \frac{s^2c^3}{8bh^3E_{11}L^2}\left[1 + 8\frac{a}{c} + 16\frac{aL}{c^2} + 32\frac{aL^2}{c^3} + 16\frac{Ls(s-4L)}{c^3}\right]$$

$$+ \frac{s[4L(2L-s) - sc]]}{8bhkG_{13}L^2} + \frac{s^2c^3}{8bh^3E_{11}L^2}$$

$$\times \left[5.07\left(\frac{h}{c}\right)\left(\frac{E_{11}}{E_{33}}\right)^{1/4} + 8.58\left(\frac{h}{c}\right)^2\left(\frac{E_{11}}{E_{33}}\right)^{1/2} + 2.08\left(\frac{h}{c}\right)^3\left(\frac{E_{11}}{E_{33}}\right)^{3/4}\right]$$

$$+ \frac{s^2c^3}{8bh^3E_{11}L^2}\left[0.98\left(\frac{h}{c}\right)\left(\frac{E_{11}}{G_{13}}\right)^{1/2} + 0.43\left(\frac{h}{c}\right)^2\left(\frac{E_{11}}{G_{13}}\right)\right]$$

$$+ \frac{1}{\pi}\frac{3s^2c^2}{4bh^2E_{11}L^2}\left(\frac{E_{11}}{G_{13}}\right)^{1/2}. \quad (35)$$

The energy release rate components by the help of Equations (27) and (28) are:

$$G_{\mathrm{I}}^{\mathrm{OLB}} = \frac{12P^2s^2c^2}{16b^2h^3E_{11}L^2}\left[1 + 0.85\left(\frac{h}{c}\right)\left(\frac{E_{11}}{E_{33}}\right)^{1/4} + 0.71\left(\frac{h}{c}\right)^2\left(\frac{E_{11}}{E_{33}}\right)^{1/2}\right.$$

$$\left. + 0.32\left(\frac{h}{c}\right)\left(\frac{E_{11}}{G_{13}}\right)^{1/2} + 0.1\left(\frac{h}{c}\right)^2\left(\frac{E_{11}}{G_{13}}\right)\right], \quad (36)$$

$$G_{\mathrm{II}}^{\mathrm{OLB}} = \frac{9P^2s^2c^2}{16b^2h^3E_{11}L^2}\left[1 + 0.22\left(\frac{h}{c}\right)\left(\frac{E_{11}}{G_{13}}\right)^{1/2} + 0.048\left(\frac{h}{c}\right)^2\left(\frac{E_{11}}{G_{13}}\right)\right], \quad (37)$$

where s is the position of the applied load from the left side of the specimen and $c = 2L - a$ is the length of the uncracked part. The total strain energy release rate ($G_{\mathrm{I/II}} = G_{\mathrm{I}} + G_{\mathrm{II}}$) can be calculated by summing Equations (33)–(34) and (36)–(37). The mixed mode-ratio ($G_{\mathrm{I}}/G_{\mathrm{II}}$) can be also computed for both specimens.

FINITE ELEMENT ANALYSIS

The FE analysis was performed using the commercial COSMOS/M 2.0 finite element package (Structural Research and Analysis Corp., 1996) to validate the beam theory-based compliance expressions. The models of the SLB and OLB specimens were built by using linear elastic PLANE2D elements under a plane strain condition. Note that the beam formulation of the problems involves a plane stress condition. The boundary conditions were the same as those illustrated in Figure 1. The specimens were loaded by a concentrated force equal to unity and the compliance of the specimens was determined in the extended ranges of the crack length (for details see the next section). The mode–mix ratio ($G_{\mathrm{I}}/G_{\mathrm{II}}$) was calculated using the virtual crack closure technique (VCCT) (Rybicki and Kanninen, 1977). At the crack tip a typical mesh (Figure 6) suggested by Davidson et al. (1996) was used. The finite crack extension was $\Delta a = 0.03125$ mm. This way it was possible to obtain elements with a size of 0.5×0.5 mm. Furthermore, the effect of the position of the applied load on the mode ratio was also studied. The elastic properties of the composite material and the geometrical parameters of the specimens are provided in the next section.
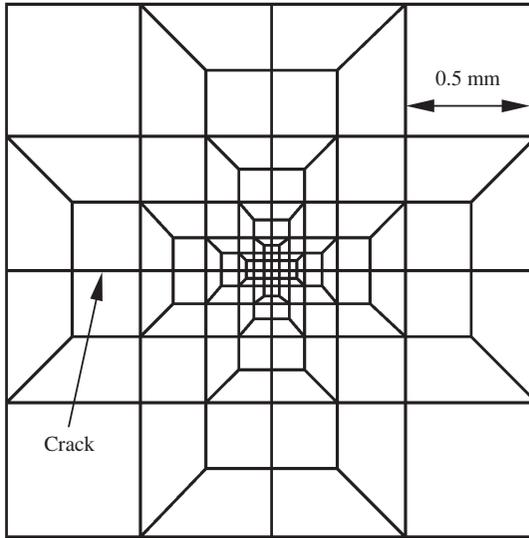
Figure 6. *FE mesh around the crack tip.*

EXPERIMENTS AND DATA REDUCTION

The constituent materials were procured from Novia Ltd. The properties of the E-glass fiber are $E = 70\,\text{GPa}$ and $\nu = 0.27$, while for the unsaturated polyester resin are $E = 3.5\,\text{GPa}$ and $\nu = 0.35$. Both were considered isotropic. The unidirectional ($[0°]_{14}$) glass/polyester specimens with a nominal thickness of $2h = 6\,\text{mm}$, a width of $b = 20\,\text{mm}$, and a fiber-volume fraction of $V_f = 43\%$ were manufactured in a special pressure tool. A great advantage of this material is the transparency, which allows for the visual observation of crack initiation/propagation. A nylon insert with a thickness of $0.03\,\text{mm}$ was placed at the midplane of the specimens to make an artificial starting defect. Then the specimens were precracked in an opening mode of 4–5 mm. The flexural modulus was determined from a three-point bending test using six uncracked specimens. The experiment resulted in $E_{11} = 33\,\text{GPa}$, additional properties were predicted by using simple rule of mixture, this way $E_{33} = 7.2\,\text{GPa}$, $G_{13} = 3\,\text{GPa}$ and $\nu_{13} = 0.27$ were obtained.

Crack initiation tests were carried out for both the SLB (Figure 7(a)) and OLB (Figure 7(b)) specimens. In the case of the SLB test the full span length was $2L = 151\,\text{mm}$. The specimens with initial crack lengths from 20 to 75 mm with 5 mm increment were prepared. For the OLB test the span length was also $2L = 151\,\text{mm}$. Furthermore, the position of the external load

was $s = 47.5$ mm. In this case the crack length ranges from 55 to 115 mm with 5 mm increment was investigated, and crack propagation tests using six specimens with $a = 50$ mm initial crack length were also performed. The tests were carried out using an Amsler testing machine under displacement control. The load–deflection data was measured. The latter was monitored by the dial gauge, shown in Figure 7. The crack length was measured visually. For this reason a millimeter scale was traced on the lateral sides of the specimens and the position of the crack tip was marked on the upper surface of the specimens. The contact regions above the supports were slightly roughened in order to prevent longitudinal sliding.

Two methods were used for data reduction: beam theory-based approach described in the 'beam theory-based analysis' section 2 and the compliance calibration (CC) (e.g., Schuecker and Davidson, 2000) method. In the case of the SLB test the experimental compliance values were fitted by the following polynomial expression (see e.g., Szekrényes and Uj, 2004):

$$C^{\text{SLB}} = C_{01} + ma^3, \tag{38}$$

where C_{01} and m were found by using least square fitting. The compliance of the OLB specimen may be found in a similar form to that of the ONF specimen (Wang et al., 2003):

$$C^{\text{OLB}} = C_{02} + n(a - 2L)^3. \tag{39}$$

The coefficients C_{02} and n were determined by least square fitting. The SERR may be calculated using Equation (2).
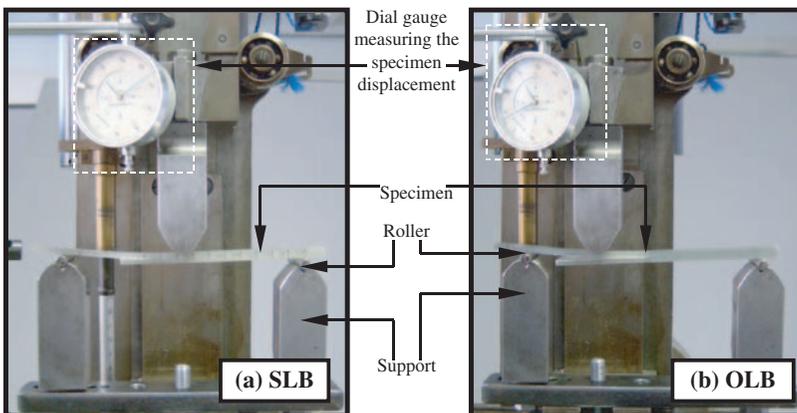
Figure 7. Single-leg bending (a) and over-leg bending (b) tests for mixed-mode I/II interlaminar fracture.

RESULTS AND DISCUSSION

Crack Initiation Tests

Figure 8 shows the load–displacement curves recorded up to fracture initiation for both specimens. Each curve is typically linear, but the two tests produce quite distinct results. For the OLB test both the critical load and displacement increase with crack length. The ranges of the applied load are essentially the same in both tests, but it should be kept in mind that the crack length ranges are different. The SLB test indicates that the critical load reaches the highest value if the crack length exhibits the lowest value
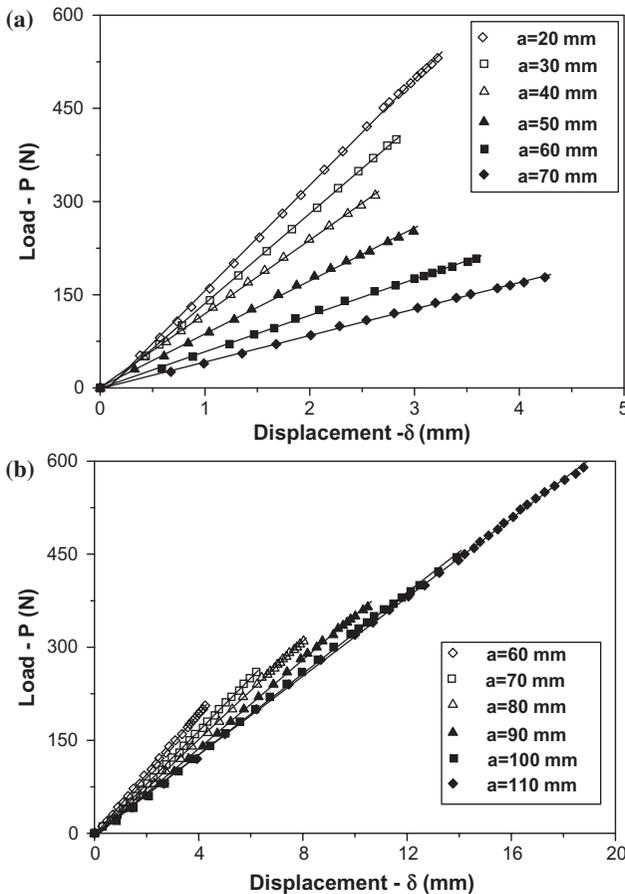
Figure 8. *Load–displacement curves up to fracture initiation: (a) SLB test and (b) OLB test.*
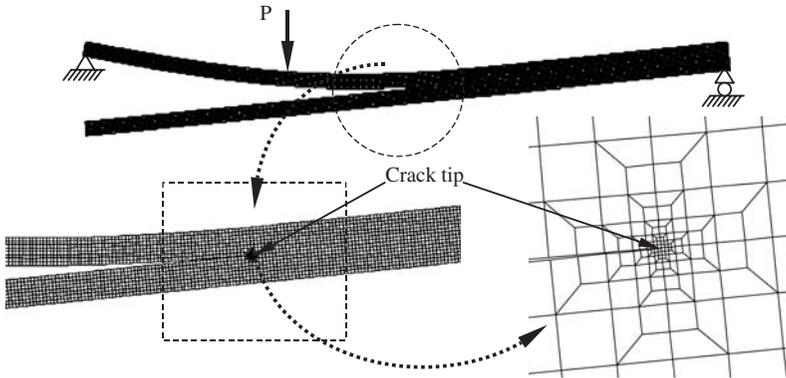
Figure 9. *Deformation of the finite element mesh, scale factor: 0.7.*

Table 1. Comparison of the results by the FE and beam models, SLB specimen.

a (mm)	20	25	30	35	40	45	50	55	60	65	70	75
C_{FE}/C_{E-B}	1.058	1.071	1.084	1.096	1.105	1.112	1.115	1.117	1.116	1.115	1.112	1.105
C_{Beam}/C_{E-B}	1.051	1.062	1.073	1.082	1.089	1.094	1.096	1.097	1.096	1.094	1.091	1.088
$(G_I/G_{II})_{Beam}$	1.675	1.604	1.557	1.524	1.499	1.480	1.465	1.453	1.443	1.434	1.427	1.420
$(G_I/G_{II})_{FE}$	1.628	1.579	1.545	1.520	1.503	1.485	1.476	1.468	1.462	1.449	1.457	1.324

a, crack length; C_{FE}, compliance, plane strain FE model; C_{Beam}, compliance, beam model, Equation (32); $(G_I/G_{II})_{Beam}$, mode mix ratio, beam model; $(G_I/G_{II})_{FE}$, mode mix ratio, plane strain FE model.

(Figure 8(a)). The results of the OLB are in sharp contrast with these facts, i.e., the critical load increases with the initial crack length.

   In Figure 9 we demonstrate the deformation of the FE mesh of the OLB specimen. The displaced shape of the SLB specimen is similar. The mesh has a high density, therefore a detailed view is included at the crack tip. The compliances calculated from the beam theory-based solution were compared with the results of the FE analysis. In each case the compliance values are normalized with the result of the EB beam theory. These are the first terms in Equations (1) and (5). Tables 1 and 2 list the normalized values of the two solutions for both configurations. Equations (32) and (35) show very good agreement with the FE results, which confirms the applicability of the analytical solution. The mode–mix ratio is also collected in Tables 1 and 2. The ratio by the FE analysis changes within 1.63–1.32 in the case of the SLB and decreases from 1.32 to 1.24 in the case of the OLB specimen. For the

Table 2. Comparison of the results by the FE and beam models, OLB specimen.

a (mm)	50	55	60	65	70	75	80	85	90	95	100	105	110	115
C_{FE}/C_{E-B}	1.127	1.102	1.082	1.067	1.055	1.046	1.039	1.033	1.028	1.024	1.021	1.018	1.015	1.013
C_{Beam}/C_{E-B}	1.108	1.084	1.068	1.056	1.046	1.039	1.033	1.029	1.025	1.021	1.018	1.016	1.014	1.012
$(G_I/G_{II})_{Beam}$	1.398	1.402	1.406	1.410	1.415	1.420	1.427	1.434	1.443	1.453	1.465	1.480	1.499	1.524
$(G_I/G_{II})_{FE}$	1.316	1.314	1.319	1.308	1.304	1.299	1.294	1.298	1.280	1.272	1.275	1.249	1.250	1.236

a, crack length; C_{FE}, compliance, plane strain FE model; C_{Beam}, compliance, beam model; C_{E-B}, compliance, beam model, Equation (35); $(G_I/G_{II})_{Beam}$, mode–mix ratio, beam model; $(G_I/G_{II})_{FE}$, mode–mix ratio, plane strain FE model.

Table 3. The effect of the position of the applied load on the mode ratio (a = 60 mm).

s (mm)	20	30	40	50	60	70	80	90	100
$(G_I/G_{II})_{FE}$	1.314	1.320	1.314	1.317	1.344	1.467	1.457	1.454	1.461

s, position of the applied load; $(G_I/G_{II})_{FE}$, mode–mix ratio, plane strain FE model.

SLB specimen the solution based on beam theory predicts values between 1.68 and 1.42 as the crack length increases. This is in excellent agreement with the VCCT method. On the other hand in the case of the OLB specimen the mode ratio by beam analysis has values between 1.4 and 1.52 with the increasing crack length. According to the VCCT method the crack length dependency of the mode–mix ratio is somewhat stronger in the case of the SLB coupon.

In order to explain the disagreement between the result of the VCCT and the beam model for the mode ratio of the OLB specimen, we performed FE analyses in which the position of the applied load was varied. Note that the crack length was held at a constant value ($a = 60$ mm). The result of the analysis is listed in Table 3. It transpires that the mode ratio is approximately constant until the position of the load reaches the crack tip. At this point it seems that there is a little transition, where the mode ratio slightly enhances. If the position of the load is higher than the position of the crack tip there is a jump in the mode ratio. It is apparent that this effect is not included in the beam model, which (assuming similar behavior at the other crack lengths) may explain the disagreement with respect to the mode ratios.

The compliance curves determined for the SLB and OLB coupons based on crack initiation tests are illustrated in Figures 10(a) and 11(a). The advanced beam model (Equation (32)) of the SLB coupon slightly overpredicts the experimental points, although the overpredictions are not significant. The slightly unusual compliance curves were calculated based on experimental data from the OLB specimens. In this case the characteristic distance c, in the beam theory solution (Equations (35), (36), and (37)), is the length of the uncracked region. In spite of this, the agreement between the result of the beam theory-based solution (Equation (35)) and the experiment is excellent. The values of the SERR at propagation onset are plotted in Figures 10(b) and 11(b). In the case of the SLB specimens the CC method results in a 645 J/m² plateau value, while the beam model predicts a 625 J/m² for the steady-state value. The results show opposite trends in the case of the OLB specimen, i.e., the beam model overpredicts the experiments. The CC method reports a 650 J/m² plateau value, while
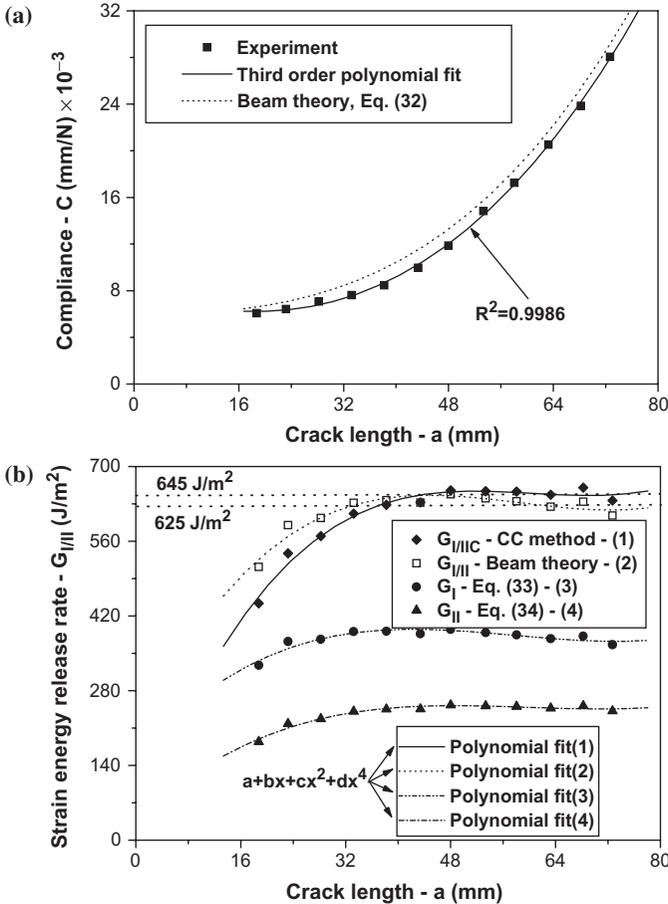
Figure 10. Compliance (a) and values of the strain energy release rate (b) against the crack length (SLB specimen).

the relevant result of the beam model is $715 \, \text{J/m}^2$ (9% difference). It should be mentioned that less than 1% difference was found between the steady-state SERR values of the SLB and OLB configurations ($645 \, \text{J/m}^2$ against $650 \, \text{J/m}^2$). Consequently, the two tests lead to essentially the same result.

In our previous work using the same material the SCB setup also resulted in a $645 \, \text{J/m}^2$ steady-state SERR value. Similar trends were also obtained by others using MMF specimens. The only difference between the MMF and SLB configurations is the distinct thicknesses above the left support. Albertsen et al. (1995) reported $G_{\text{I/II, init}} = 145 \, \text{J/m}^2$ initiation and
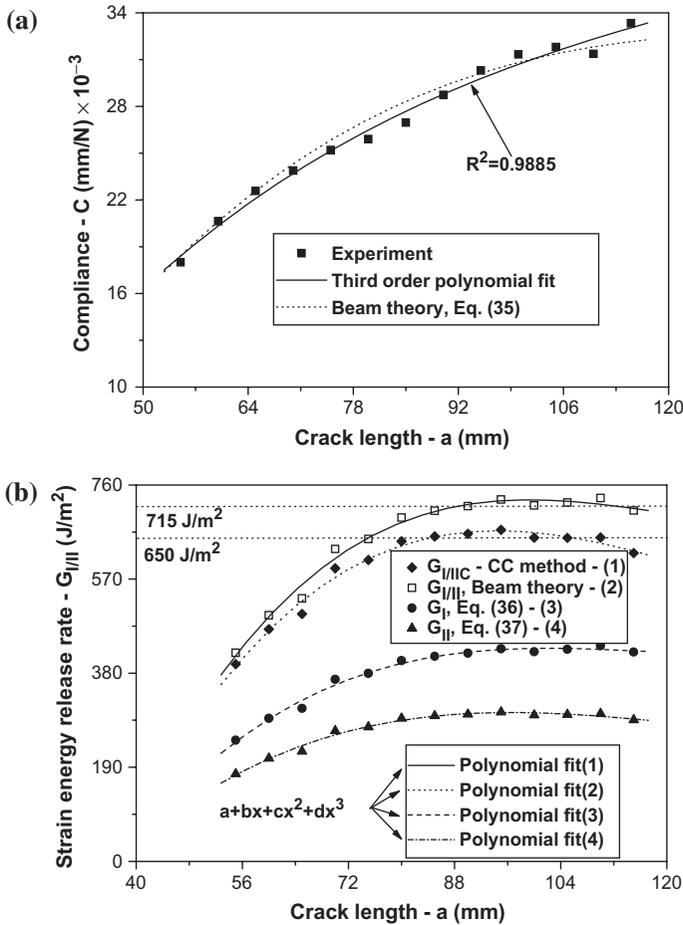
Figure 11. *Compliance (a) and values of the strain energy release rate (b) against the crack length (OLB specimen).*

$G_{\text{I/II, ss}} = 330\,\text{J/m}^2$ mean propagation values for carbon-fiber reinforced MMF specimens. In the work of Korjakin et al. (1998) the relevant values were $G_{\text{I/II, init}} = 456\,\text{J/m}^2$ and $G_{\text{I/II, ss}} = 525\,\text{J/m}^2$ for glass/epoxy MMF specimens. The character of the SERR followed the same trend as is found in Figures 10(a) and 11(a).

The values of the critical load and critical displacements up to propagation onset (or crack initiation) are illustrated in Figure 12(a). An immediate observation is that the load values recorded during the SLB test follow a hyperbolic character, while the load values from the OLB test increase with crack length. The critical displacement (Figure 12(b)) in
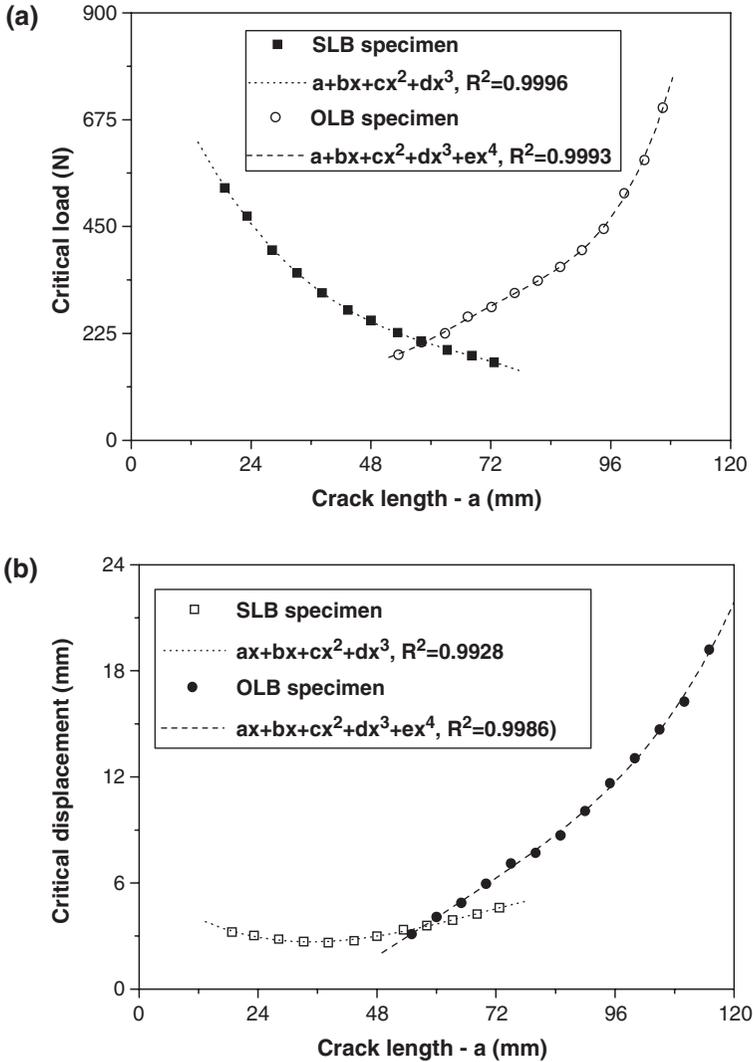
Figure 12. *The critical load (a) and the critical displacement (b) against the crack length.*

the SLB test reaches its lowest value at $a = 40$ mm. On the other hand the displacement increases dramatically if the results of the OLB test are considered. The measured load and displacement values against the crack length in each case may fit very well by using third-and fourth-order polynomials, as shown in Figure 12(a) and 12(b).

Crack Propagation Tests

Under the current geometrical parameters the SLB specimens were not suitable for propagation tests. At shorter crack lengths ($a = 20$ to 45 mm) sudden jumps (15 to 30 mm) in the crack advance frequently occurred. The remaining interval (until the point of load introduction) was insufficient for studying crack propagation. Therefore, the OLB test was used as a candidate to examine mixed-mode crack propagation. The compliance curves of each six specimens were essentially the same as those determined through the initiation test (Figure 11(a)). The load–displacement curves of six specimens are depicted in Figure 13(a). The range of the applied load is eventually the same as those which were recorded during initiation tests (Figure 8(b)). The crack initiation always occurred at $P = 170$ to 180 N.

The propagation R-curves are plotted in Figure 13(b) and (c). Although six specimens were tested, the results of only two specimens are displayed. The curves show the R-curve behavior, i.e., there is not a clear plateau value. Overall the SERR grows up to 1250 J/m^2. The agreement between the result of the CC method and beam theory is also good. Note that fiber-bridging was observed during testing, although this effect was not considered here. Furthermore, due to the relatively small displacements before the crack tip region, the significance of this phenomen was estimated to be small. The extension of the fiber-bridging was only mild in each specimen. The tested specimens at the end of the delamination process are shown in Figure 14. The initially curved crack front became curved after crack propagation onset.

For comparison, Tracy et al. (2003) determined similar propagation R-curves with 1500 and 1750 J/m^2 plateau values using the proposed SFPLB configuration with carbon/epoxy specimens to those, shown in Figure 13. Beam theory-based equations were used for data reduction in their study.

CONCLUSIONS

Under the current geometry and material the traditional SLB configuration was only suitable to investigate the crack initiation in the material. An over-leg bending (OLB) delamination specimen is proposed in the present work, which was shown to be a useful tool to evaluate mixed-mode I/II crack propagation in composites with relatively low flexural modulus. The applicability of the OLB setup was demonstrated by using unidirectional E-glass/polyester composite. In addition, closed-form solutions for the compliance and the strain energy release rates were derived based on linear beam theories.
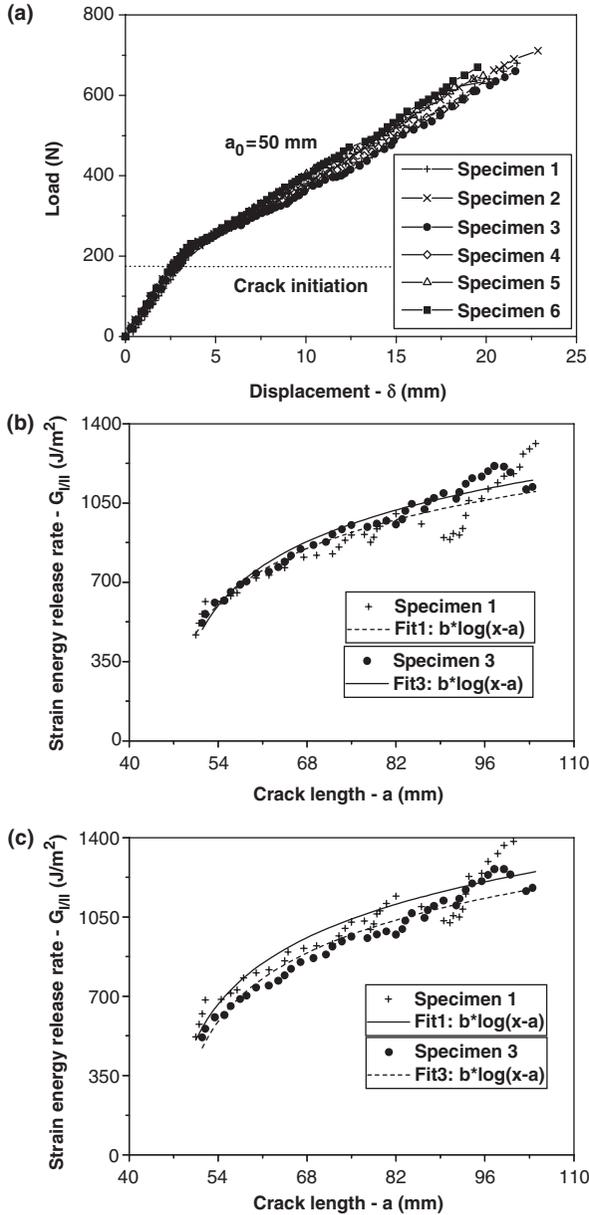
Figure 13. *Load–displacement curves from the test of six OLB specimens (a). Energy release rate against the crack length: CC method (b) and beam theory (c).*
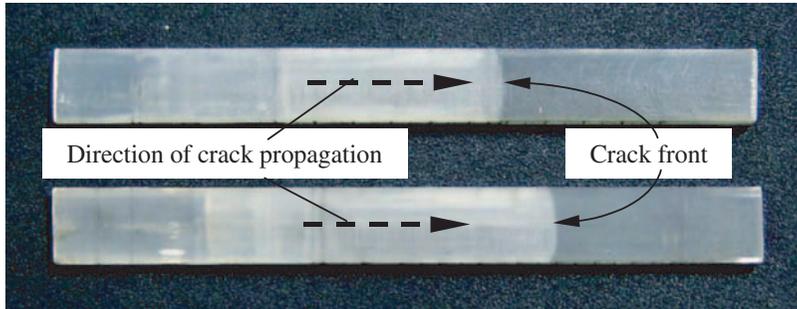
Figure 14. *Fractured specimens at the end of the delaminaton process.*

The crack initiation tests were performed utilizing the SLB and OLB setups. In both cases quite good agreement was established between the experimentally and analytically determined compliance values. Considering the steady-state value of the SERR at crack initiation, the two tests produce values within 1% difference ($645\,J/m^2$ against $650\,J/m^2$). The *R*-curves (under crack propagation) were determined using the new configuration based on two reduction schemes, and good agreement was found. This indicates that the used beam model can be applied for data reduction.

In the OLB test the large displacements do not influence the crack propagation and the propagation can be easily controlled. Moreover, the test essentially gives linear elastic response, and simple reduction technique (CC method) applies for data evaluation. The OLB coupon promotes more stable crack propagation than the SLB due to the possibility of greater crack length. A relative drawback of the OLB setup is that the mode ratio may be changed (similarly to the SLB and SCB coupons) only in a small degree.

REFERENCES

Albertsen, H., Ivens, J., Peters, P., Wevers, M. and Verpoest, I. (1995). Interlaminar Fracture Toughness of CFRP Influenced by Fiber Surface Treatment, Part I. Experimental results, *Composites Science and Technology*, **54**: 133–145.

Bradley, W.L. and Cohen, R.N. (1985). Matrix Deformation and Fracture in Graphite-reinforced Epoxies, In: Johnson, W.S. (ed.), *Delamination and Debonding of Materials*, ASTM STP 876, pp. 389–410.

Carlsson, L.A., Gillespie, Jr., J.W. and Pipes, R.B. (1986). On the Analysis and Design of the End Notched Flexure (ENF) Specimen for Mode II Testing, *Journal of Composite Materials*, **20**: 594–604.

Chatterje, S.N. (1991). Analysis of Test Specimens for Interlaminar Mode II Fracture Toughness, Part 1: Elastic laminates, *Journal of Composite Materials*, **25**: 470–493.

Davidson, B.D., Krüger, R. and König, M. (1995). Three-dimensional Analysis of Center-delaminated Unidirectional and Multidirectional Single-leg Bending Specimens, *Composites Science and Technology*, **54**: 385–394.

Davidson, B.D. and Sundararaman, V. (1996). A Single Leg Bending test for Interfacial Fracture Toughness Determination, *International Journal of Fracture*, **78**: 193–210.

Davidson, B.D., Fariello, P.L., Hudson, R.C. and Sundararaman V. (1997). Accuracy Assessment of the Singular-field-based Mode-mix Decomposition Procedure for the Prediction of Delamination, *Composite Materials: Testing and Design*, 13th Volume, ASTM STP 1242, pp. 109–128.

Davidson, B.D. and Koudela, K.L. (1999). Influence of the Mode Mix of Precracking on the Delamination Toughness of Laminated Composites. *Journal of Reinforced Plastics and Composites*, **18**: 1408–1414.

Davidson, B.D., Gharibian, S.J. and Yu, L. (2000). Evaluation of Energy Release Rate-based Approaches for Predicting Delamination growth in Laminated Composites. *International Journal of Fracture*, **105**: 343–365.

Davies, P., Ducept, F., Brunner, A.J., Blackman, B.R.K. and de Morais, A.B. (1996). Development of a standard mode II Shear fracture Test Procedure, In: *Proceedings of the 7th European Conference on Composite Materials*, (ECCM-7) London, May Vol. 2, pp. 9–15.

Davies, P., Casari, P. and Carlsson, L.A. (2004). Influence of Fiber Volume Fraction on the Interlaminar Fracture Toughness of glass/epoxy using the 4ENF specimen, *Composites Science and Technology*, **65**: 295–300.

Ding, W. and Kortschot, M.T. (1999). A Simplified Beam Analysis of the End Notched Flexure Mode II Delamination Specimen, *Composite Structures*, **45**: 271–278.

Ducept, F., Gamby, D. and Davies, P. (1999). A Mixed-mode Failure Criterion Derived from Tests of Symmertic and Asymmetric Specimens, *Composites Science and Technology*, **59**: 609–619.

Hashemi, S., Kinloch, J. and Williams, J.G. (1990a). The Effects of Geometry, Rate and Temperature on Mode I, Mode II and Mixed-mode I/II Interlaminar Fracture Toughness of Carbon-fibre/poly(ether-ether ketone) Composites, *Journal of Composite Materials*, **24**: 918–956.

Hashemi, S., Kinloch, J. and Williams, J.G. (1990b). Mechanics and Mechanisms of Delamination in a Poly(ether sulphone)-fibre Composites, *Composites Science and Technology*, **37**: 429–462.

Korjakin, A., Rikards, R., Buchholz, F.-G., Wang, H., Bledzki, A.K. and Kessler, A. (1998). Comparative Study of Interlaminar Fracture Toughness of GFRP with Different Fiber Surface Treatments, *Polymer Composites*, **19**(6): 793–806.

Morais, de A.B., Moura, de M.F., Marques, A.T. and Castro, de P.T. (2002). Mode-I Interlaminar Fracture of Carbon/Epoxy Cross-ply Composites, *Composites Science and Technology*, **62**: 679–686.

Olsson, R. (1992). A Simplified Improved Beam Analysis of the DCB Specimen, *Composites Science and Technology*, **43**: 329–338.

Ozdil, F., Carlsson, L.A. and Davies, P. (1998). Beam Analysis of Angle-ply Laminate End-notched Flexure Specimens. *Composites Science and Technology*, **58**: 1929–1938.

Ozdil, F. and Carlsson, L.A. (1999). Beam Analysis of Angle-ply Laminate Mixed-mode Bending Specimens, *Composites Science and Technology*, **59**: 937–945.

Pagano, N.J. and Schoeppner, G.A. (2000). Delamination of Polymer Matrix Composites: Problems and Assessment, In: Kelly, A. and Zweben, C. (eds), *Comprehensive Composite Materials*, Vol. 2, pp. 433–528, Oxford, Elsevier Science.

Pieracci, A., Davidson, B.D. and Sundararaman, V. (1998). Nonlinear Analyses of Homogeneous, Symetrically Delaminated Single Leg Bending Specimens, *Journal of Composites Technology and Research*, **20**(3): 170–178.

Polaha, J.J., Davidson, B.D., Hudson, R.C. and Pieracci, A. (1996). Effects of Mode Ratio, Ply Orientation and Precracking on the Delamination Toughness of a Laminated Composite, *Journal of Reinforced Plastics and Composites*, **15**: 141–173.

Qiao, P., Wang, J. and Davalos, J.F. (2004). Analysis of Tapered ENF Specimen and Characterization of Bonded Interface Fracture under Mode-II Loading, *International Journal of Solids and Structures*, **40**: 1865–1884.

Qiao, P. and Wang, J. (2004). Mechanics and Fracture of Crack-tip Deformable Bimaterial Interface, *International Journal of Solids and Structures*, **41**: 7423–7444.

Reeder, J.R. and Crews, Jr., J.H. (1990). Mixed-mode Bending Method for Delamination Testing, *AIAA Journal*, **28**(7): 1270–1276.

Russel, A.J. and Street, K.N. (1985). Moisture and Temperature Effects on the Mixed-mode Delamination Fracture of Unidirectional Graphite/Epoxy, In: Johnson, W.S. (ed.), *Delamination and Debonding of Materials*, American Society for Testing and Materials, Philadelphia, ASTM STP 876, pp. 349–370.

Rybicki, E.F. and Kanninen, M.F. (1977). A Finite Element Calculation of Stress Intensity Factors by a Modified Crack Closure Integral, *Engineering Fracture Mechanics*, **9**: 931–938.

Schuecker, C. and Davidson, B.D. (2000). Evaluation of the Accuracy of the Four-point Bend End-notched Flexure Test for Mode II Delamination Toughness Determination, *Composites Science and Technology*, **60**: 2137–2146.

Structural Research and Analysis Corp. (1996). COSMOS/M 2.0 Complete Finite Element Documentation.

Suo, Z. and Hutchinson, J.W. (1990). Interface Crack between Two Elastic Layers, *International Journal of Fracture*, **43**: 1–18.

Szekrényes, A. and Uj, J. (2004). Beam and Finite Element Analysis of Quasi-Unidirectional SLB and ELS Specimens, *Composites Science and Technology*, **64**: 2393–2406.

Szekrényes, A. and Uj, J. (2005a). Comparison of Some Improved Solutions for Mixed-mode Composite Delamination Coupons, *Composite Structures* (to appear, available at www.sciencedirect.com).

Szekrényes, A. and Uj, J. (2005b). Mode-II Fracture in E-Glass/Polyester Composite, *Journal of Composite Materials*, **39**(19): 1747–1768.

Szekrényes, A. and Uj, J. (2005c). An Improved Analytical Delamination Model for Unidirectional Specimens, *Mechanical of Materials* (submitted for publication).

Tanaka, K., Yuasa, T. and Katsura, K. (1998). Continuous Mode II Interlaminar Fracture Toughness Measurement by Over Notched Flexure Test, In: *Proceedings of the 4th European Conference on Composites: Testing and Standardization*, pp. 171–179.

Tay, T.E. (2003). Characterization and Analysis of Delamination Fracture in Composites – an overview of developments from 1990 to 2001, *Applied Mechanics Reviews*, **56**(1): 1–32.

Tracy, G.D., Feraboli, P. and Kedward, K.T. (2003). A New Mixed Mode Test for Carbon/Epoxy Composite Systems, *Composites Part A: Applied Science and Manufacturing*, **34**: 1125–1131.

Wang, H. and Vu-Khanh, T. (1996). Use of End-loaded-split (ELS) Test to Study Stable Fracture Behaviour of Composites under Mode-II Loading, *Composite Structures*, **36**: 71–79.

Wang, J. and Qiao, P. (2003). Fracture Toughness of Wood-Wood and Wood-FRP Bonded Interfaces under Mode-II Loading, *Journal of Composite Materials*, **37**(10): 875–897.

Wang, J. and Qiao, P. (2004a). Novel Beam Analysis of the End Notched Flexure Specimen for Mode-II Fracture, *Engineering Fracture Mechanics*, **71**: 219–231.

Wang, J. and Qiao, P. (2004b). Interface Crack between two Shear Deformable elastic layers, *Journal of the Mechanics and Physics of Solids*, **52**: 891–905.

Wang, W.-X., Takao, Y. and Nakata M. (2003). Effects of Friction on the Measurement of the Mode II Interlaminar Fracture Toughness of Composite Laminates, In: *Proceedings of the 14th International Conference on Composite Materials*, San Diego, California, USA, July, pp. 14–18.

Williams, J.G. (1988). On the Calculation of Energy Release Rates for Cracked Laminates, *International Journal of Fracture*, **36**: 101–119.

Williams, J.G. (1989). End Corrections for Orthotropic DCB Specimens, *Composites Science and Technology*, **35**: 367–376.

Yang, Z. and Sun, C.T. (2000). Interlaminar Fracture Toughness of a Graphite/epoxy Multidirectional Composite, *Journal of Engineering Materials and Technology*, **122**: 428–433.

Yoon, S. H. and Hong, C.S. (1990). Modified End Notched Flexure Specimen for Mixed Mode Interlaminar Fracture in Laminated Composites, *International Journal of Fracture*, **43**: R3–R9.